Role of Ion Pairing in Double-Layer Effects at Self-Assembled Monolayers Containing a Simple Redox Couple

Rafael Andreu,* Juan Jose Calvente, W. Ronald Fawcett,*,† and Miguel Molero

Departamento de Química Física, Facultad de Química, Universidad de Sevilla, 41012 Sevilla, Spain

Received: November 5, 1996; In Final Form: January 20, 1997[⊗]

The influence of ion pairing on the potential distribution at an electrode modified with a redox-active self-assembled monolayer is considered. The voltammetric response of the film is modeled as a function of its dielectric properties and the extent of association between the redox centers and counterions in solution. On the basis of the scheme of squares, a general treatment for any number of association steps is introduced. In addition, the effect of the counterion selective permeation on the voltammetric features is presented. It is shown that ion pairing and double-layer effects are strongly coupled, and may lead in some situations to the same variation of the peak potential with electrolyte concentration. The possibility of obtaining association parameters from voltammetric experiments is discussed. Comparison is made with Rowe and Creager's data on the oxidation of mixed monolayers of ferrocene-*n*-hexanethiol and *n*-alkanethiols.

Introduction

Interest in double-layer effects at self-assembled monolayers (SAM) on metal electrodes dates from the seminal work of Smith and White.[1,2] They pointed out that the electrostatic potential experienced by a charged head group in such a monolayer depends on the dielectric properties of the interfacial region, the charge on the electrode, and the ionic strength. As a result, when a redox couple is incorporated in the SAM, the position and shape of the cyclic voltammogram involving the redox process depend on the electrostatic potential at the head group.

Studies of medium effects on the thermodynamics of redox processes involving ferrocene head groups immersed in an alkanelike environment were carried out by Rowe and Creager.[3−5] These authors found that the peak potential for the oxidation of the bound ferrocene to ferrocinium cation depends on the nature and concentration of the anion in the bulk electrolyte and concluded that ion pairing plays a significant role in the overall oxidation process. Electrochemical quartz crystal microbalance measurements of the mass changes accompanying the oxidation of surface attached ferrocene[6,7] and viologen[8] groups suggest the presence of a reversible anion association process. More recently, Redepenning and Flood[9] analyzed the dependence of the formal potential for ferrocenylhexanethiol monolayers in $HClO_4$ aqueous solution on electrolyte activity and concluded that the monolayer is strongly associated with perchlorate anions in the oxidized state. Additional evidence for the presence of ion pairing has been reported for SAMs with incorporated Ru(III)/Ru(II)[10] and Os(III)/Os(II)[11] redox centers. The general picture which emerges from this work is that ion pairing should be considered in evaluating double-layer effects on self-assembled redox systems.

In the present paper, the work of Smith and White[1] is extended to examine the effects of ion pairing on the reactions undergone by redox centers incorporated in SAMs. The coupling between ion pairing and double-layer structure is examined in some detail. Use is made of a traditional mean field theory of the interface in which the SAM contributes a region of low permittivity between the metal electrode and the electrolyte solution. Though mean field theories often involve a simplified picture of real systems, they provide a necessary reference framework, before attempting further improvements of the model, to include discreteness of charge effects, monolayer heterogeneity, or finite ion sizes, for instance.

Theory

Coupling between Ion Pairing and Potential Distribution. Adsorption of an organic monolayer on a metallic electrode results in a region of low dielectric permittivity, which extends from the electrode surface to the plane of closest approach of solvated ions in solution (Figure 1). This low dielectric permittivity ϵ_a is typically in the range 2−8 for alkanethiol monolayers.[12] In addition, this region also includes a layer of solvent molecules contacting the organic adsorbate whose structure is different from that of the bulk solvent.

We consider the monolayer to be a mixture of electroactive and nonelectroactive organic molecules of similar structure. Electroactive adsorbates include a redox group, which may exchange electrons with the electrode. The total surface concentration of redox sites will be denoted by Γ_T. They are assumed to be located on a plane, at a distance β from the electrode surface, and therefore they are all equivalent from an electrostatic point of view. While the electrolyte ions are not allowed to enter the inner part of the monolayer ($0 \le x \le \beta$), the outer region of low permittivity ($\beta \le x \le \beta + \gamma$) is considered to be either a perfect (Figure 1a) or a selective (Figure 1b) barrier toward ion permeation. In the later case, only counterions of the redox centers populate the outer region of the monolayer, without modifying its dielectric properties. We denote by γ_A the distance between the plane of the redox sites and the plane of closest approach of the counterions, so that $\gamma_A = \gamma$ for a perfect barrier and $\gamma_A < \gamma$ for a selective barrier.

Beyond the low-permittivity region, the diffuse layer is described according to Gouy−Chapman theory.[13]

Consider now the electron exchange between the electrode and the surface-attached redox couple:

$$O^{z_O} + ne^- \leftrightarrows R^{z_R} \qquad (1)$$

† Permanent address: Department of Chemistry, University of California, Davis, CA 95616.

[⊗] Abstract published in *Advance ACS Abstracts,* March 1, 1997.

S1089-5647(96)03701-7 CCC: $14.00

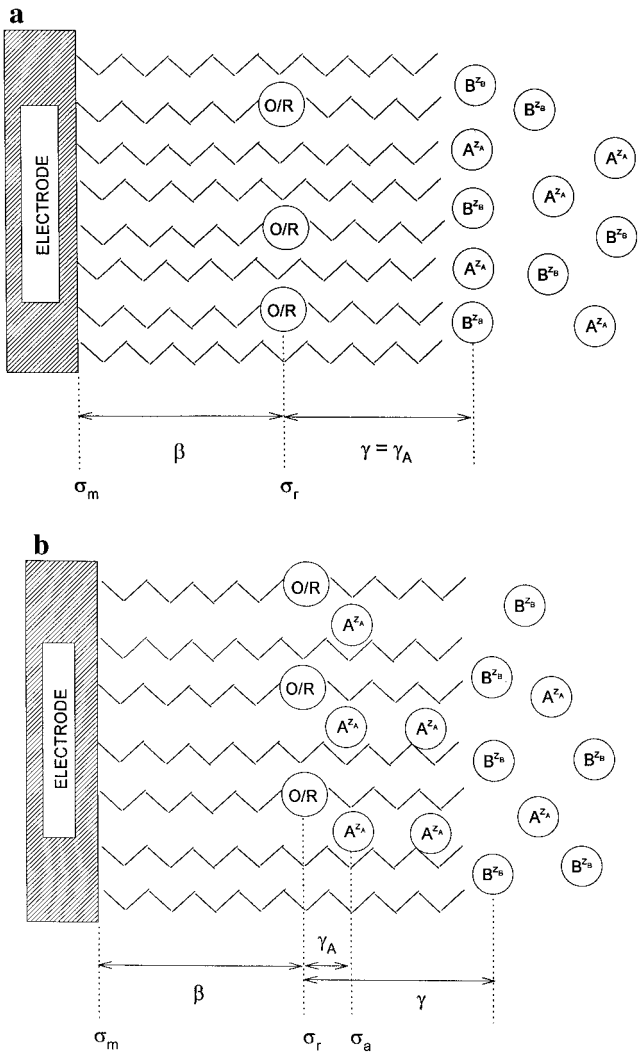

Figure 1. Schematic representation of a redox SAM attached to an electrode surface in contact with an aqueous electrolyte solution. Redox groups are denoted by O/R, electrolyte counterions by A^{zA}, and coions by B^{zB}. (a) Electrolyte ions cannot permeate the monolayer. (b) Counterions A^{zA} can enter the outer part of the adsorbed monolayer.

Under equilibrium conditions, one may write

$$\bar{\mu}_O + n\bar{\mu}_e = \bar{\mu}_R \tag{2}$$

where $\bar{\mu}_i$ is the electrochemical potential of the i-species (i = O or R), which can be split into chemical and electrical terms,

$$\bar{\mu}_O = \mu_O^o + RT \ln \Gamma_O + z_O F\phi^r \tag{3}$$

$$\bar{\mu}_e = \mu_e^o - F\phi^m \tag{4}$$

$$\bar{\mu}_R = \mu_R^o + RT \ln \Gamma_R + z_R F\phi^r \tag{5}$$

Γ_i is the surface concentration of species i and ϕ^m and ϕ^r are the average electrostatic potentials on the electrode and at the plane of redox sites, respectively. Both are referenced to the mean electrostatic potential in the solution bulk; the μ_i^o's are the standard electrochemical potentials.

Substituting eqs 3−5 into eq 2, one obtains

$$\phi^m = \phi_o^m + \phi^r + \frac{RT}{nF} \ln \frac{\theta_O}{\theta_R} \tag{6}$$

where

$$\phi_o^m = \frac{\mu_O^o + n\mu_e^o - \mu_R^o}{nF} \tag{7}$$

and

$$\theta_i = \frac{\Gamma_i}{\Gamma_T} \qquad i = O, R \tag{8}$$

When species O and R can associate with ion A in solution, two additional equilibria have to be considered:

$$O^{z_O} + A^{z_A} \leftrightarrows OA^{z_O + z_A} \tag{9}$$

$$R^{z_R} + A^{z_A} \leftrightarrows RA^{z_R + z_A} \tag{10}$$

so that one may write,

$$\bar{\mu}_O + \bar{\mu}_A = \bar{\mu}_{OA} \tag{11}$$

$$\bar{\mu}_R + \bar{\mu}_A = \bar{\mu}_{RA} \tag{12}$$

As before, the chemical and electrical contributions to $\bar{\mu}_A$, $\bar{\mu}_{OA}$, and $\bar{\mu}_{RA}$ can be made explicit to obtain

$$\bar{\mu}_A = \mu_A^o + RT \ln c_A \tag{13}$$

$$\bar{\mu}_{OA} = \mu_{OA}^o + RT \ln \Gamma_{OA} + F(z_O\phi^r + z_A\phi^A) \tag{14}$$

$$\bar{\mu}_{RA} = \mu_{RA}^o + RT \ln \Gamma_{RA} + F(z_R\phi^r + z_A\phi^A) \tag{15}$$

where c_A is the bulk concentration of A and ϕ^A is the potential at the plane of closest approach of A. Therefore, the ion pair is modeled as two point charges (z_O, z_A or z_R, z_A) at a distance γ_A from each other. Note that γ_A is not necessarily zero (or $\phi^r = \phi^A$) to form an ion pair, although γ_A values greater than a few hundred picometers are not expected to lead to significant ion pairing.

Substituting eqs 3, 13, and 14 into eq 11, and eqs 5, 13, and 15 into eq 2, one obtains

$$\ln(K_O c_A) = \frac{z_A F\phi^A}{RT} + \ln \frac{\theta_{OA}}{\theta_O} \tag{16}$$

$$\ln(K_R c_A) = \frac{z_A F\phi^A}{RT} + \ln \frac{\theta_{RA}}{\theta_R} \tag{17}$$

Equations 6, 16, 17, and the following identity:

$$\theta_O + \theta_R + \theta_{OA} + \theta_{RA} = 1 \tag{18}$$

provide the basic link between electrode potential and redox conversion. In terms of surface coverages, the charge density at the plane of the redox centers σ_r is given by

$$\sigma_r = F\Gamma_T\{z_O(\theta_O + \theta_{OA}) + z_R(\theta_R + \theta_{RA})\} \tag{19}$$

and that at the plane $x = \beta + \gamma_A$, due to the counterions which are associated to the redox centers, it is

$$\sigma_A = z_A F\Gamma_T(\theta_{OA} + \theta_{RA}) \tag{20}$$

To proceed further, one has to relate ϕ^m, ϕ^r, and ϕ^A to the geometrical and dielectric characteristics of the system. By applying Gauss' law (see ref 1) one obtains

$$\phi^m = \frac{\sigma_m \beta}{\epsilon_o \epsilon_a} + \frac{(\sigma_m + \sigma_r)\gamma_A}{\epsilon_o \epsilon_a} + \phi^A \tag{21}$$

and

$$\phi^r = \frac{(\sigma_m + \sigma_r)\gamma_A}{\epsilon_o \epsilon_a} + \phi^A \tag{22}$$

where σ_m is the charge density on the metal. The latter quantity can be expressed in terms of the surface coverages combining eqs 6, 21, and 22:

$$\phi_m = \frac{\epsilon_o \epsilon_a}{\beta}\left[\phi_o^m + \frac{RT}{nF} \ln \frac{\theta_O}{\theta_R}\right] \tag{23}$$

Two alternatives are considered to estimate ϕ^A, depending on whether A can permeate the outer region of the monolayer or not.

(a) When the organic adsorbate behaves as a perfect barrier against ion A, $\gamma_A = \gamma$, it is assumed that cations and anions share a common plane of closest approach. According to Gouy−Chapman theory[13] for 1:1 electrolytes, or their mixtures,

$$\phi^A = \frac{2RT}{F} \sinh^{-1}\left(\frac{\sigma_m + \sigma_r + \sigma_A}{2B}\right) \tag{24}$$

where $B = (2RT\epsilon_s\epsilon_o c_b)^{1/2}$, ϵ_s being the relative permittivity of the solvent and c_b the solution ionic strength. Therefore, ion pairing modifies the value of ϕ^A, as eq 24 shows clearly.

(b) When the counterion A permeates through the outer region of the monolayer, $\gamma > \gamma_A$, the plane of closest approach of A is located at a distance $\beta + \gamma_A$ from the electrode surface, while the plane of closest approach of nonpermeating ions is at $\beta + \gamma$. Though there is not a simple analytical expression for ϕ^A, its value can be obtained from the modified Gouy−Chapman theory with unequal distances of closest approach of the electrolyte ions (MGC/UDCA).[14,15] The use of this theory represents a purely electrostatic approach to describe ion partition between two phases with different dielectric properties: the outer part of the organic monolayer and the solution, thereby neglecting any change in the chemical contribution to the solvation energy of the counterion.

The potential $\phi(x)$ at a plane parallel to the electrode is computed by solving the Poisson−Boltzmann equation, under some restrictions imposed by the space regions accessible to each ion.

(I) For $\beta + \gamma_A \le x \le \gamma + \beta$

$$\frac{d^2\phi}{dx^2} = -\frac{F}{\epsilon_o \epsilon_a} z_A c_A \exp(-z_A F\phi/RT) \tag{25}$$

with the following boundary conditions:

$$\left(\frac{d\phi}{dx}\right)_{x=\beta+\gamma_A} = -\frac{1}{\epsilon_o \epsilon_a}(\sigma_m + \sigma_r + \sigma_A) \tag{26}$$

and

$$\epsilon_a\left(\frac{d\phi}{dx}\right)_{x=(\beta+\gamma)_-} = \epsilon_s\left(\frac{d\phi}{dx}\right)_{x=(\beta+\gamma)_+} \tag{27}$$

(II) For $x \ge \gamma + \beta$

$$\frac{d^2\phi}{dx^2} = -\frac{F}{\epsilon_o \epsilon_s}\sum_i z_i c_i \exp(-z_i F\phi/RT) \tag{28}$$

with the boundary conditions:

$$\phi(\infty) = \left(\frac{d\phi}{dx}\right)_{x=\infty} = 0 \tag{29}$$

and

$$\phi(\beta + \gamma)_+ = \phi(\beta + \gamma)_- = \phi(\beta + \gamma) \tag{30}$$

where $\phi(\beta + \gamma)$ is determined as follows. First, eq 28 is solved with an initial guess of $\phi(\beta + \gamma)$ to obtain $(d\phi/dx)_{x = (\beta+\gamma)+}$. By using the continuity of the electric displacement at $x = (\beta + \gamma)$ given by eq 27, eq 25 is integrated to compute $(d\phi/dx)_{x=\beta+\gamma_A}$. This value is compared with the right hand side of eq 26. The above procedure is iteratively repeated for several $\phi(\beta + \gamma)$ values until eq 26 is satisfied.[15]

Voltammetric Response. In the previous set of equations, the parameters describing the system are ϵ_a, ϵ_s, T, ϕ_o^m, Γ_T, K_O, K_R, z_O, z_R, c_A, c_b, γ, γ_A, and β. However, most of them can be obtained independently, as will be discussed later. The unknown variables are θ_O, θ_R, θ_{OA}, θ_{RA}, and σ_m; ϕ^m is taken as the independent variable. For given values of the parameters the unknown variables are calculated as follows.

Let ρ be the ratio θ_O/θ_R, so that

$$\theta_O = \rho\theta_R \tag{31}$$

By subtracting eq 16 from eq 17 and rearranging, one obtains

$$\theta_{OA} = \rho\frac{K_O}{K_R}\theta_{RA} \tag{32}$$

Combining eqs 18, 31, and 32, the following expression for θ_{RA} results:

$$\theta_{RA} = \frac{K_R}{K_R + \rho K_O}[1 - (1 + \rho)\theta_R] \tag{33}$$

Combining eqs 33 and 17, one obtains

$$\frac{K_R}{K_R + \rho K_O}[1 - (1 + \rho)\theta_R] = \theta_R K_R c_A \exp\left(-\frac{z_A F\phi^A}{RT}\right) \tag{34}$$

Substituting eqs 31−33 into eqs 19, 20, and 23, σ_m, σ_r, and σ_a can be expressed in terms of ρ and θ_R:

$$\sigma_m = \frac{\epsilon_o \epsilon_a}{\beta}\left[\phi_o^m + \frac{RT}{nF} \ln \rho\right] \tag{35}$$

$$\sigma_r = \frac{F\Gamma_T}{K_R + \rho K_O}[\rho n(K_R - K_O)\theta_R + z_R K_R + z_O K_O \rho] \tag{36}$$

$$\sigma_A = z_A F\Gamma_T[1 - (1 + \rho)\theta_R] \tag{37}$$

Therefore, in this way the unknown variables have been expressed as a function of ρ and θ_R. For a given value of ρ, eq 34 is iteratively solved for θ_R. In each iteration ϕ^A is calculated by using one of the two alternatives mentioned in the previous section. The required σ_m, σ_r, and σ_a values are determined by using eqs 35−37. Once θ_R has been calculated, θ_O, θ_{OA}, and θ_{RA} are determined from eqs 31−33. Finally, the potential on the metal ϕ^m is obtained by using eq 21. This process is then

repeated for a different value of ρ to obtain θ_R, θ_O, θ_{OA}, and θ_{RA} as a function of ϕ^m.

The current measured in a voltammetric experiment is the sum of charging (i_c) and faradaic (i_f) components,

$$i_T = i_f + i_c \tag{38}$$

The faradaic current, due to the flow of electrons between the redox centers and the electrode, is given by

$$i_f = nFS\Gamma_T \frac{d(\theta_O + \theta_{OA})}{dt} \tag{39}$$

where S is the electrode area and t the elapsed time. If the potential is scanned at a constant rate υ,

$$i_f = nFS\Gamma_T \upsilon \frac{d(\theta_O + \theta_{OA})}{d\phi^m} \tag{40}$$

The charging current is directly related to the interfacial capacitance (C_d):

$$i_c = \upsilon S C_d \tag{41}$$

which is defined as

$$C_d = \left(\frac{\partial \sigma_m}{\partial \sigma^m}\right)_{\mu_i,T} \tag{42}$$

Therefore, the overall current may be expressed as

$$i_T = \upsilon S\left(nF\Gamma_T \frac{d(\theta_O + \theta_{OA})}{d\phi^m} + \frac{\partial \sigma_m}{\partial \phi^m}\right) \tag{43}$$

Theoretical voltammograms are obtained by numerical differentiation of ($\theta_O + \theta_{OA}$) and σ_m with respect to ϕ^m.

Results and Discussion

As indicated above, electrostatic modeling of redox monolayers requires a large set of parameters. In an experimental situation, there is likely to be some uncertainty associated to the actual value of the interfacial parameters. Fortunately, ellipsometric[16] and capacitance[17] measurements allow assignment of ϵ_a and $\beta + \gamma$ values within a reasonable range of error. On the other hand, much less is known about γ_A, so that it may be considered as an adjustable parameter, whose values are bounded between zero (by the present model) and a distance comparable to typical molecular diameters. Therefore, we will present first results for the $\gamma_A = 0$ case, and consider later the influence of $\gamma_A > 0$.

a. Ions A Can Enter the Plane of the Redox Centers ($\gamma_A = 0$). It may be also convenient to split this section into two parts, according to the relative position of the plane through the redox centers and the monolayer/solution boundary.

a.1. Redox Centers Placed at the End of the Organic Monolayer ($\gamma = 0$). In this case the diffuse layer extends up to the redox plane which is in contact with all ions in solution. In the absence of ion pairing the voltammetric response of this system has been described by Smith and White.[1] As may be anticipated, ion-pairing has a dramatic influence on the interfacial potential distribution and the shape of the voltammetric waves. Figures 2 and 3 show the effect of K_O on an adsorbed redox couple under conditions which are representative of a ferrocene monolayer ($\Gamma_T = 3 \times 10^{-10}$ mol cm^{-2}, $z_O = +1$, $z_R = 0$, and $K_R = 0$). As K_O increases, the voltammetric peaks become narrower and, eventually, shift toward more negative

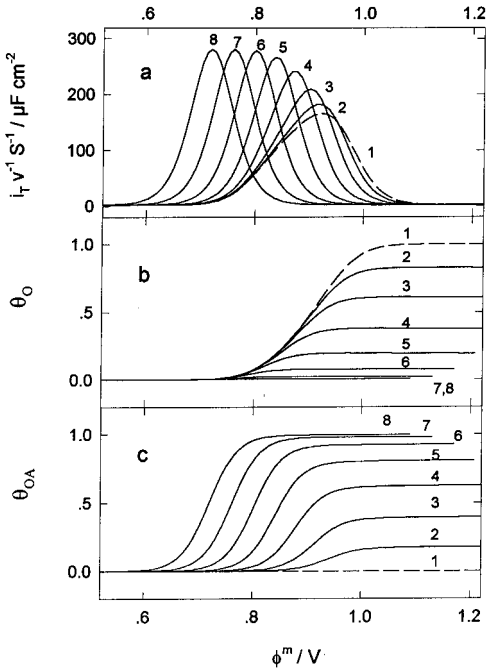

Figure 2. (a) Simulated voltammograms, (b) surface coverage of the free oxidized form, and (c) surface coverage of ion-paired oxidized form as a function of applied potential. Broken-line curves were computed in the absence of ion pairing. Full-line curves correspond to the following values of K_O: (2) 0.01, (3) 0.05, (4) 0.25, (5) 1.25, (6) 6.25, (7) 31.25, and (8) 156.25 M^{-1}. Other parameter values were $\beta = 15$ Å, $\gamma = \gamma_A = 0$, $\epsilon_a = 3$, $\epsilon_s = 78$, $\Gamma_T = 3 \times 10^{-10}$ mol cm^{-2}, $c_A = c_b = 1$ M, $z_O = +1$, $z_R = 0$, $z_A = -1$, $K_R = 0$, and $\phi_o^m = 0.85$ V.

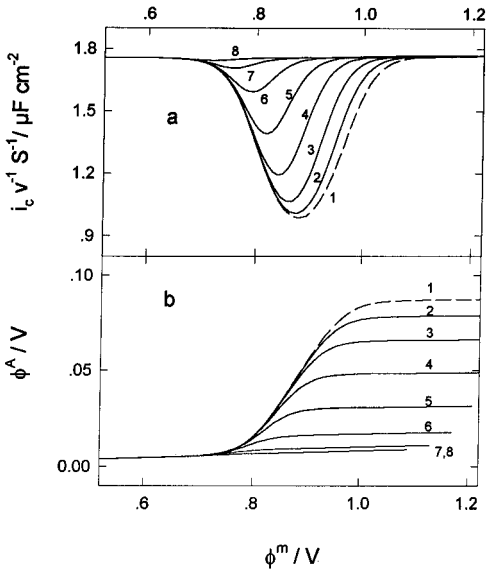

Figure 3. (a) Nonfaradaic contribution to the voltammogram and (b) potential at the redox centers plane as a function of applied potential. Symbols and parameter values as in Figure 2.

potentials at a rate close to 59 mV/K_O decade. Under these last conditions, $\theta_O \ll \theta_{OA}$ (compare Figures 2b,c), the faradaic current is given by

$$i_f = FS\Gamma_T \upsilon \frac{d\theta_{OA}}{d\phi^m} \tag{44}$$

To show explicitely the relationship between θ_{OA} and ϕ^m, eq 6 may be rewritten as follows:

$$\phi^m = \left(\phi_o^m - \frac{RT}{F} \ln K_O c_A\right) + (\phi^r + z_A \phi^A) + \frac{RT}{F} \ln \frac{\theta_{OA}}{\theta_R} \tag{45}$$

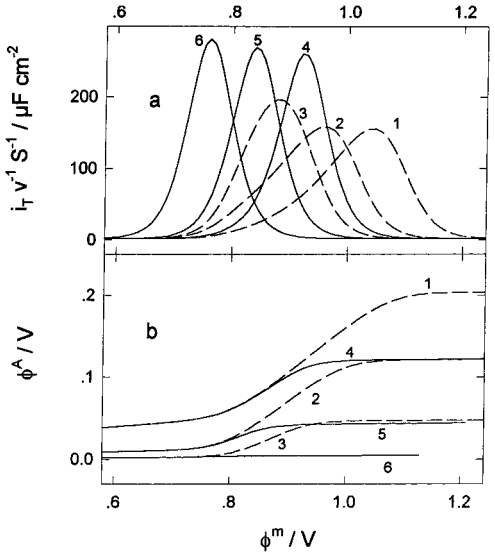

Figure 4. (a) Simulated voltammograms as a function of electrolyte concentration in the absence (− −) and the presence (—, $K_O = 5\ M^{-1}$, $c_A = c_b$) of ion pairing. Electrolyte concentration: 0.01 M (curves 1 and 4), 0.25 M (curves 2 and 5), and 6.25 M (curves 3 and 6). (b) Potential at the plane through the redox centers as a function of the applied potential for the same conditions as (a). Other parameter values as in Figure 2.

where the first term within brackets is the apparent formal potential for the OA/R redox couple, and the second term within brackets gives rise to the double-layer contribution to the faradaic current. When $z_O = -z_A$ and $z_R = 0$, as in the ferrocinium/ferrocene case interacting with a monovalent anion, extensive ion pairing leads to $\sigma_r + \sigma_a \approx 0$ and ϕ^A is determined by σ_m, the dielectric properties of the interphase and the bulk solution composition. For the β and ϵ_a values that apply to these systems, most of the potential drop occurs between the metal and the plane of the redox centers and ϕ^A becomes very small, so that

$$i_c \approx \upsilon S \frac{\epsilon_o \epsilon_a}{\beta} \tag{46}$$

The set of eqs 44−46 predict a voltammetric response identical to that originally derived for adsorbed redox couples in the absence of double layer effects.[18] However, the apparent formal potential depends now on the value of $K_O c_A$.

By comparing Figures 2b,c, it may be observed that θ_O decreases upon increasing K_O, while θ_{OA} not only increases, but also moves toward more negative potentials, being responsible for the shift of the whole voltammogram. As OA and R are uncharged species for this particular system, the variation of θ_O with ϕ^m also determines the nonfaradaic contribution to the overall current (Figure 3a).

Experimental evidence for ion pairing is usually obtained from the shift of the peak potential with the counterion concentration. If the ionic strength is kept constant, or high enough, by addition of an inert electrolyte, variations of K_O or c_A have the same effect on the voltammogram, and a peak shift of 59 mV/c_A decade is a good indication of the presence of ion pairing. However, if c_A and ionic strength are varied simultaneously, one must be aware of the changes of the diffuse layer potential that may contribute significantly to the peak shift.

Figure 4a shows the expected voltammetric behavior for 25-fold changes in electrolyte concentration, in the absence (broken lines) and presence (full lines) of ion pairing. In both cases, peak potentials become more negative at a rate of 59 mV/ concentration decade. In the absence of ion pairing, the peak shift originates in the electrolyte concentration dependence of ϕ^A. This can be shown by recalling that, at the voltammetric peak potential, $\theta_O \approx \theta_R \approx 0.5$ and $(\sigma_r)_{peak} \approx (z_O + z_R)F\Gamma_T/2$, so that by combining eqs 6 and 24, one obtains

$$\phi_{peak} \approx \phi_o^m + \frac{2RT}{F} \sinh^{-1}\left(\frac{(\sigma_m + \sigma_r)_{peak}}{2B^* c_b^{1/2}}\right) \tag{47}$$

where $B^* c_b^{1/2} = B$ in eq 24. When the redox coverage is high enough ($\Gamma_T \geq 10^{-10}$ mol cm^{-2}), $|(\sigma_r)_{peak}| \gg |\sigma_m|$, $|(\sigma_r)_{peak}| \gg 2B^* c_b^{1/2}$, and the concentration dependence of ϕ_{peak} may be approximated by

$$\phi_{peak} = \text{const} - \frac{RT}{F} \ln c_b \tag{48}$$

Therefore, when $c_A = c_b$, one cannot distinguish between ion pairing (eq 45) and double-layer effects (eq 48) only from the variation of ϕ_{peak} with electrolyte concentration.

The higher ϕ^A values, characteristic of dilute electrolyte solutions, act as ion pairing promoters (see eq 16). A comparison of curve 3 in Figure 2a and curve 4 in Figure 4a, both computed with $K_O c_A = 0.05$, reveals a higher degree of ion pairing in the second case, as indicated by a narrower and higher voltammogram.

When both forms of the redox couple bear a net charge, one should consider the simultaneous influence of $|z_O| + |z_R|$ ion pairing equilibria. Working equations to obtain the voltammetric response in the presence of any number of association equilibria have been derived in Appendix A. Under extensive ion pairing conditions (i.e., $K_{O,i}$, $K_{R,i} \rightarrow \infty$) each oxidized and reduced center retains $|z_O|$ and $|z_R|$ counterions, respectively, to form ionic aggregates which are electrically neutral. No further association is assumed for the neutral aggregates. It follows that

$$\theta_O + \sum_i \theta_{OA_i} \approx \theta_{OA_{|z_O|}} \tag{49}$$

and

$$\theta_R + \sum_i \theta_{RA_i} \approx \theta_{RA_{|z_R|}} \tag{50}$$

so that $\sigma_a + \sigma_r \approx 0$. Equation 6 can be combined with eqs A.11−A.14 to give

$$\phi^m = \left[\phi_o^m + \frac{RT}{nF} \ln \frac{\prod_{k=1}^{|z_R|} K_{R,k}}{\prod_{k=1}^{|z_O|} K_{O,k}} - \frac{|z_O| - |z_R|}{n} \frac{RT}{F} \ln c_A\right] + \left[\frac{|z_O| - |z_R|}{n} z_A \phi^A + \phi^r\right] + \frac{RT}{nF} \ln \frac{\theta_{OA_{z_O}}}{\theta_{RA_{z_R}}} \tag{51}$$

The redox conversion takes place between neutral ion pairs and, as indicated before, ϕ^A and ϕ^r are identical and very small when

SCHEME 1

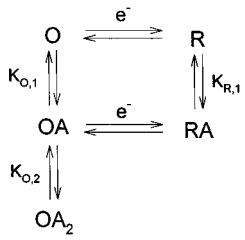

$\gamma_A = 0$. Then the current reaches its maximum value at

$$(\phi^m)_{peak} = \left[\phi_o^m + \frac{RT}{nF}\ln\frac{\prod_{k=1}^{|z_R|}K_{R,k}}{\prod_{k=1}^{|z_O|}K_{O,k}}\right] - \frac{|z_O| - |z_R|}{n}\frac{RT}{F}\ln c_A \quad (52)$$

It is noted that $(\phi^m)_{peak}$ may shift toward either more positive or negative potentials on increasing c_A, according to the relative values of $|z_O|$ and $|z_R|$. The shape of the voltammetric wave is again identical to that derived for a reversible redox couple, with both forms adsorbed under langmuirian conditions.[18]

Under less extensive ion-pairing conditions, the analysis of a given experimental system may become prohibitively involved as the number of association steps increases. To alleviate this problem, it seems advisable to adopt some simplifying assumptions. For instance, association constants are expected to increase with the charge of the ionic species involved. This hypothesis finds some support in the observed increase of acid/base association constants by a factor > 100 when the charge on the acceptor molecule is made one unit more negative.[19] From a purely electrostatic point of view, one would expect that association constants involving equally charged species would have similar values. However, it is also likely that steric effects would tend to decrease the association constants of those equilibria that accumulate a larger number of counterions on the redox center.

To illustrate the transition from extensive to negligible ion pairing, consider a +2/+1 redox couple, for which three association constants $K_{O,1}$, $K_{O,2}$, and $K_{R,1}$ are defined according to Scheme 1.

Figure 5a shows how the shape of the voltammogram is independent of ionic strength and the peak shift is controlled by c_A under strong ion-pairing conditions. Figure 5c displays the opposite situation where ion pairing is weak and the peak shift is determined by the ionic strength of the electrolyte solution. For intermediate values of the association constants (Figure 5b), voltammograms obtained in the presence of a single salt solution retain the 59 mV/decade shift due to the diffuse layer potential and are very similar to those in Figure 5a. On the other hand, voltammograms in Figure 5b corresponding to fixed ionic strength solutions evolve from the weak ion-pairing shape to the strong ion-pairing shape on increasing c_A, but at a rate smaller than 59 mV/decade.

a.2. Redox Centers Embedded in the Monolayer (γ > 0). Up to now, the condition $\gamma_A = \gamma = 0$ has been considered. This situation corresponds to redox groups attached at the end of the monolayer, so that they are in close contact with the electrolyte solution. However, the redox centers are often embedded in the organic monolayer, so that a region of low permittivity is situated between the redox centers and the solution. There is some evidence[20] indicating that this region may act as a selective barrier, preventing the approach of some electrolyte ions according to their hydrophilicity. Some results

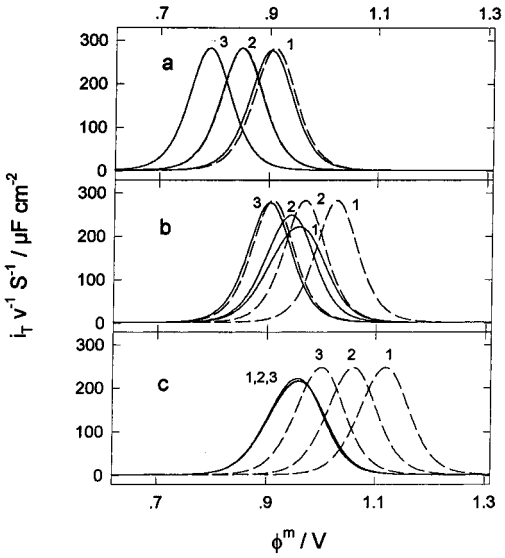

Figure 5. Theoretical voltammograms of a +2/+1 redox couple as a function of association constant values and electrolyte composition: (—) Fixed ionic strength, $c_b = 1$ M, and (– –) variable ionic strength, $c_b = c_A$; (1) $c_A = 0.001$ M, (2) $c_A = 0.01$ M, (3) $c_A = 0.1$ M. Association constant values: (a) $K_{O,1} = 100$ M^{-1}, $K_{O,2} = K_{R,1} = 0.1$ M^{-1}, (b) $K_{O,1} = 1$ M^{-1}, $K_{O,2} = K_{R,1} = 10^{-3}$ M^{-1}, and (c) $K_{O,1} = 10^{-2}$ M^{-1} and $K_{O,2} = K_{R,1} = 10^{-5}$ M^{-1}. Other parameter values as in Figure 2. Theoretical voltammograms for fixed and variable ionic strength overlap in curves 2a and 3a.

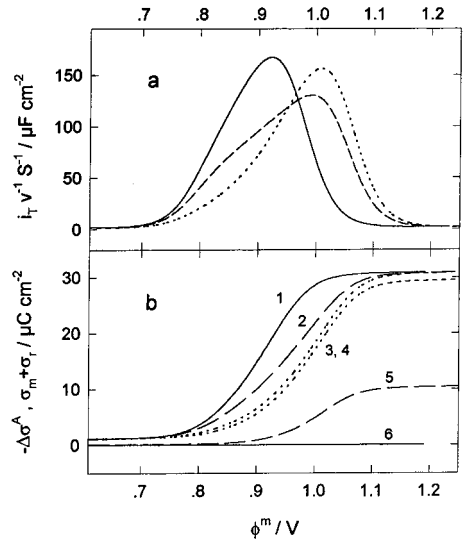

Figure 6. (a) Theoretical voltammograms as a function of thickness of the outer region of the monolayer γ: (—) 0 Å, (– –) 0.1 Å, and (•••) ≥1 Å. $K_O = K_R = \gamma_A = 0$ and other parameter values as in Figure 2. (b) Sum of the charge density at the metal and redox planes, $\sigma_m + \sigma_r$, curves (1, 2, and 3); and charge density due to counterions in the outer region of the monolayer $\Delta\sigma^A$, curves (4, 5, and 6). Line symbols as in (a).

for the case in which the counterions A can permeate the outer region of the monolayer ($\gamma_A = 0$ and $\gamma > 0$) are now presented. The case of a monolayer acting as a perfect barrier against ion permeation will be postponed to the next section.

The presence of a low-permittivity region, which can be populated only by counterions, is likely to cause significant changes in the potential profile of the interface. Thus, the manner in which these changes affect the voltammetric wave in the absence of ion pairing are described first.

Increasing the thickness of the outer region of the monolayer γ induces a broadening of the voltammetric wave and a displacement of the peak potential (Figure 6a). It is also observed that a further increase in the monolayer thickness

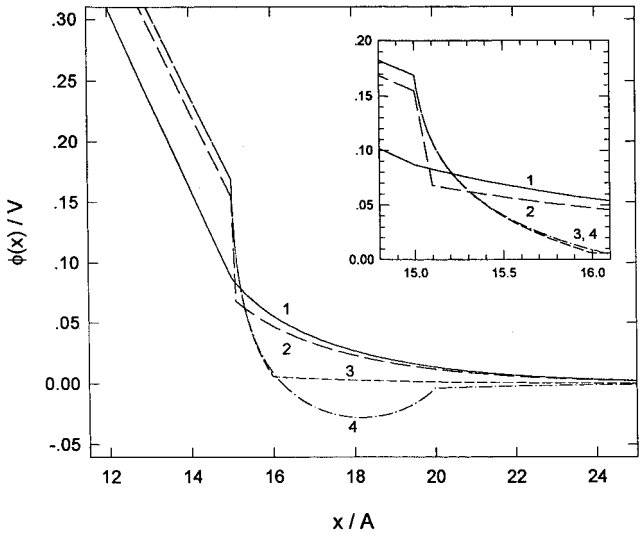

Figure 7. Potential profiles of a redox SAM as a function of γ: (1) 0, (2) 0.1, (3) 1, and (4) 5 Å. All profiles were computed at $\phi^m = 1.2$ V. The redox centers plane is located at 15 Å from the metal surface. Other parameters values as in Figure 6. The inset shows a blow up of the region around the redox centers plane.

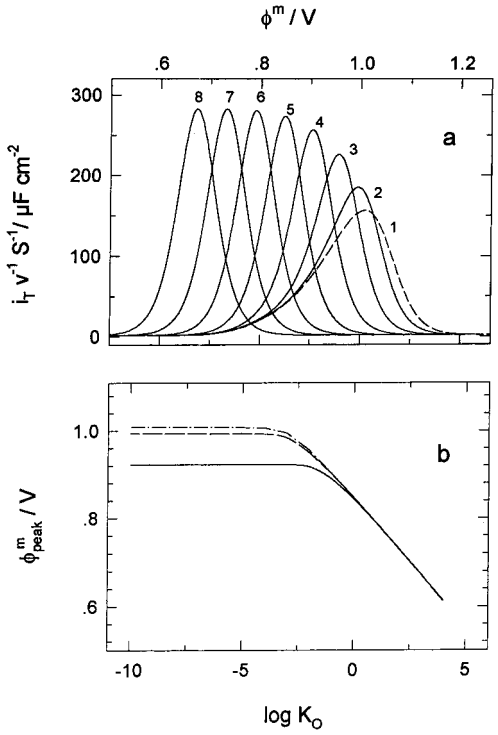

Figure 8. (a) Theoretical voltammograms for a +1/0 redox couple as a function of the association constant K_O: (1) 0, (2) 10^{-3}, (3) 10^{-2}, (4) 10^{-1}, (5) 1, (6) 10, (7) 10^2, and (8) 10^3 M^{-1}. $\gamma = 5$ Å and other parameter values as in Figure 6. (b) Shift of the peak potential with the logarithm of the association constant for several values of γ: (—) 0, (− −) 0.1, and (−·−) ≥ 1 Å.

beyond a rather small critical value ($\gamma \approx 1$ Å for the redox system in Figure 6) does not modify the voltammetric wave any more.

The origin of this particular behavior may be found in Figure 6b. As γ increases, more counterions can be accomodated in the low dielectric permittivity layer of thickness γ close to the redox centers. When γ reaches its critical value, the charge density due to the counterions in the outer region of the monolayer ($\Delta\sigma^A$) is big enough to counterbalance the charge on the metal and the redox centers. From this point, a further increase of γ results only in a very small increase of $\Delta\sigma^A$, since $|\Delta\sigma^A| > \sigma_r + \sigma_m$ and the potential inside the low permittivity region reaches negative values with respect to the solution bulk (Figure 7). Now, the potential profile in the vicinity of the redox centers does not vary any longer with γ, although the minimun displayed in curve 4 of Figure 7 becomes progressively deeper and moves away from the redox plane with increasing γ. It should be noted that the location of this minimum in the potential profile divides the interface into two electrically neutral regions.

The presence of a low-permittivity region accessible only to counterions also affects the ion-pairing equilibrium. The electrostatic interaction between charges on the metal and the redox planes and counterions are enhanced, resulting in an increase of the counterion concentration on the redox plane. Figure 8a illustrates for a +1/0 redox couple the evolution of the voltammetric wave as K_O increases when $\gamma = 5$ Å. If a comparison is made with Figure 2a ($\gamma = 0$), the main difference lies in the K_O range where the onset of extensive ion-pairing can be observed. The higher ϕ^A values obtained when the redox center is embedded in the monolayer lead to extensive ion-pairing behavior for K_O values ≈100 times smaller than in the $\gamma = 0$ case.

Figure 8b shows the expected variation of the peak potential with K_O when the γ value is varied from 0 to ∞. The fact that the voltammetric wave is independent of γ, for any γ value of practical interest, makes unneccessary a precise knowledge of this parameter in order to analyze the voltammetric response of a given experimental system. On the other hand, the dependence of peak potential and voltammetric shape on electrolyte composition is entirely analogous to that described in the previous section, though one must be aware of the changes in ϕ^A brought about by the presence of the outer part of the organic monolayer.

b. Counterions A Cannot Enter the Redox Plane ($\gamma_A > 0$). Well-organized organic monolayers have been shown to be effective barriers against permeation of hydrophilic ions.[17,18] Therefore, when redox centers are embedded within the monolayer, one would expect the outer part of the monolayer to prevent hydrophilic counterions reaching the redox plane. Also, from a more fundamental point of view, steric restrictions imposed by the finite size of the ions involved in the ion-pair equilibrium may determine a nonzero distance of closest approach of the counterions to the redox plane.

The presence of a charge free region between the redox centers and the plane of closest approach of the electrolyte ions is expected to have a strong influence on the shape of the voltammetric wave, as discussed earlier by Smith and White.[1] Under these conditions, $\phi^r \neq \phi^A$ and

$$\phi^r - \phi^A = \frac{(\sigma_m + \sigma_r)\gamma_A}{\epsilon_o \epsilon_a} \tag{53}$$

The overall potential drop at the interphase may then be expressed as

$$\phi^m = (\phi^m - \phi^r) + (\phi^r - \phi^A) + \phi^A \tag{54}$$

where only the first term on the right-hand side drives the redox conversion (eq 6). It becomes evident that, for a given value of the externally applied potential ϕ^m, ($\phi^m - \phi^r$) decreases on increasing ($\phi^r - \phi^A$) and larger overpotential values are required to reach a full conversion of the redox centers. For high redox coverages ($\Gamma_T > 10^{-10}$ mol cm^{-2}), rather small γ_A values (∼1 Å) are enough to produce drawn out voltammograms, which may extend over more than 1 V along the potential axis. Full width at half maximum ($\Delta\phi_{fwhm}$) values in the 100−200 mV

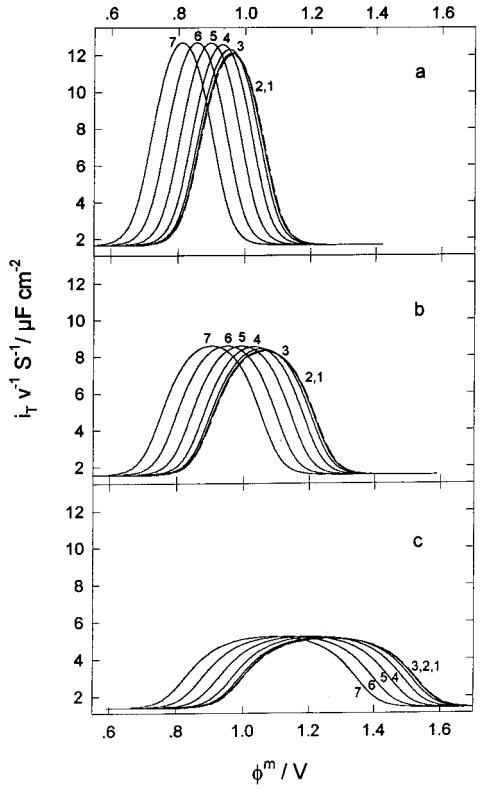

Figure 9. Theoretical voltammograms for a +1/0 redox couple as a function of K_O: (1) 0, broken line; (2) 0.05; (3) 0.25; (4) 1.25; (5) 6.25; (6) 31.25; (7) 156.25 M^{-1}. With $\gamma = \gamma_A$: (a) 1, (b) 2, and (c) 4. $\Gamma_T = 2.4 \times 10^{-11}$ mol cm^{-2}, other parameter values as in Figure 2.

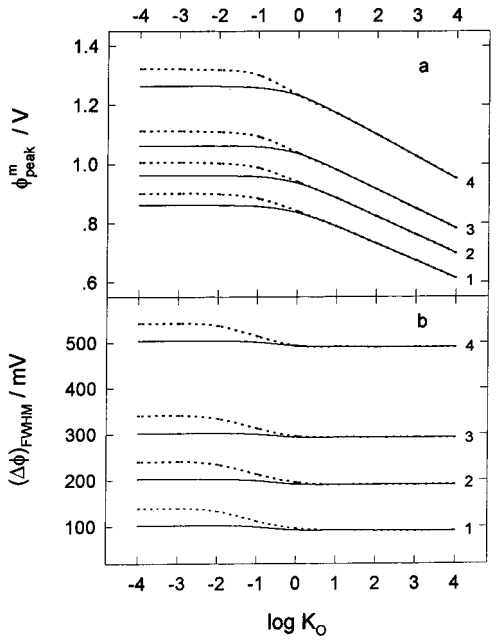

Figure 10. Variation of (a) ϕ^m_{peak} and (b) $(\Delta\phi)_{fwhm}$ as a function of the association constant of the oxidized form, for several values of γ_A: (1) 0, (2) 1, (3) 2, (4) 4 Å. Full lines correspond to $\gamma = \gamma_A$ and broken lines to the $\gamma \gg \gamma_A$ limit. $\Gamma_T = 2.4 \times 10^{-11}$ mol cm^{-2}. Other parameter values as in Figure 2.

range, as often observed experimentally, are predicted for moderate redox coverages and a γ_A/ϵ_a ratio of the order of 100 ppm.

Besides modifying the shape of the voltammetric wave, an increase in γ_A also results in a shift of the peak potential, as may be observed in Figures 9 and 10. For $\gamma_A > 0$, the presence of extensive ion pairing has only a moderate effect on the $\Delta\phi_{fwhm}$ value, which is dominated by the γ_A/ϵ_a ratio for a given redox coverage.

As was discussed before for the $\gamma_A = 0$ case, the presence of a low-permittivity region accessible only to counterions ($\gamma > \gamma_A$) has a significant influence on the voltammetric wave only when ion pairing is weak or negligible (Figure 10). Under these circumstances, it originates a further shift of the peak potential and an enlargement of the wave along the potential axis.

c. Ion Pairing in Mixed Electrolyte Solutions. An effective way of disentangling diffuse layer and ion-pairing effects on the peak potential shifts, induced by changes in electrolyte composition, seems to be the use of mixed electrolyte solutions. Ideally, the concentration of an "inert" electrolyte would be kept at a high value, while the concentration of an ion-pairing "active" electrolyte is varied from a trace level to a value close to the inert electrolyte concentration. In this way, the diffuse layer potential becomes nearly independent of the electrolyte composition, and peak shifts may be interpreted in terms of ion pairing between the redox centers and counterions delivered by the active electrolyte. An additional benifit of this approach comes from minimization of changes in liquid junction potentials and activity coefficients.

Presently, there is no evidence to support the existence of an inert counterion which does not form ion pairs with a charged monolayer. Therefore, it seems preferable to assume that any counterion present in solution may associate with the redox centers. Adopting this hypothesis implies that only relative values of the association constants and lower limits of the formal potential will be obtained from the analysis of voltammetric experiments. Working equations for the case that two counterions (A and W) can form ion pairs with the redox centers have been derived and are available as Supporting Information. A rather simple expression can be obtained for the peak potential corresponding to a +1/0 redox couple by assuming that the reduced form is not involved in association equilibria and that at the peak potential $\theta_O + \theta_{OA} + \theta_{OW} = \theta_R = 0.5$,

$$\phi^m_{peak} = \phi^m_o + \phi^r - \frac{RT}{F}\ln(1 + \lambda_{OA} + \lambda_{OW}) \qquad (55)$$

where

$$\lambda_{OA} = c_A K_{OA} \exp(-z_A F\phi^A/RT) \qquad (56)$$

$$\lambda_{OW} = c_W K_{OW} \exp(-z_W F\phi^A/RT) \qquad (57)$$

If either λ_{OA} or λ_{OW} are $\ll 1$, ϕ^m_o becomes accessible from the peak potential determined in the presence of the weakly associated electrolyte. Otherwise, only a lower limit for ϕ^m_o can be derived from the $\lambda_{OA}, \lambda_{OW} \geq 0$ condition. When both counterions are strongly associated, so that $\lambda_{OA}, \lambda_{OW} \gg 1$, the ratio K_{OA}/K_{OW} can be estimated by comparing, for instance, the peak potentials obtained in solutions with only A or W at the same concentration. Since for $\lambda_{OA}, \lambda_{OW} \gg 1$ ϕ^A becomes very small, the exponential terms in eqs 56 and 57 are close to 1, and the difference between the peak potentials may be approximated by

$$(\phi^m_{peak})_A - (\phi^m_{peak})_W = (\phi^r_{peak})_A - (\phi^r_{peak})_W + \frac{RT}{F}\ln\frac{K_{OW}}{K_{OA}} \qquad (58)$$

Moreover, if γ_A/ϵ_a is small enough, then $(\phi^r_{peak})_A \approx (\phi^r_{peak})_W$ (see eq 53) and the ratio of the two association constants may be obtained by simply comparing the two peak potentials.

d. Comparison with Experiment. Rowe and Creager[4] have reported a detailed experimental study of the influence of ion pairing on the electrochemistry of mixed monolayers of ferrocenyl-*n*-hexanethiol and *n*-alkanethiols. By analyzing the shift

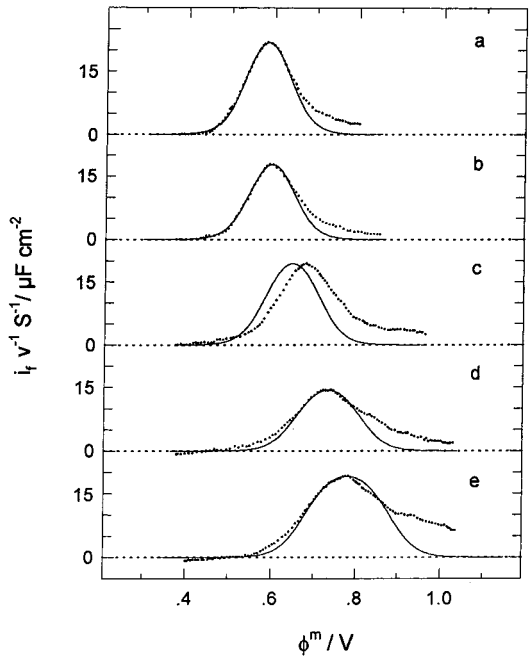

Figure 11. Faradaic component of the ferrocinium/ferrocene voltammetric wave in 1 M $HClO_4$. Ferrocenylhexanethiol was coadsorbed with (a) *n*-butanethiol, (b) *n*-hexanethiol, (c) *n*-octanethiol, (d) *n*-decanethiol, and (e) *n*-dodecanethiol. (···) Experimental data extracted from voltammograms in ref 4 by subtracting the capacitative current of the reduced monolayer; (—) theoretical values computed as indicated in the text.

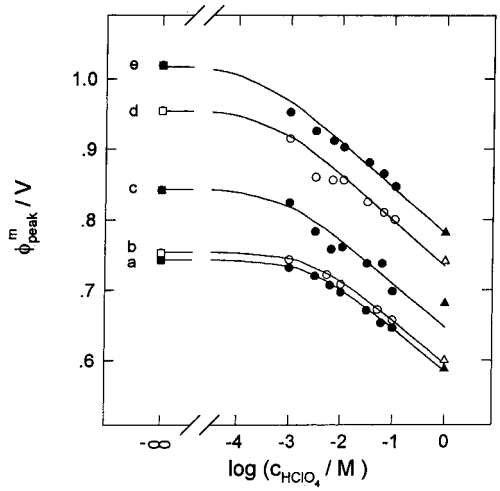

Figure 12. Variation of the ferrocinium/ferrocene peak potential with electrolyte composition (□, ■) 1 M H_2SO_4, (○, ●) 1 M H_2SO_4 + *x* M $HClO_4$, and (△, ▲) 1 M $HClO_4$. An arbitrary abscissae of 10^{-6} M has been assigned to the peak potentials in 1 M H_2SO_4 for simplicity. Separate plots correspond to the following coadsorbates: (a) *n*-butanethiol, (b) *n*-hexanethiol, (c) *n*-octanethiol, (d) *n*-decanethiol, and (e) *n*-dodecanethiol. Points are experimental values from ref 4; lines are theoretical fits computed as indicated in the text.

of the ferrocinium/ferrocene voltammetric peak with the electrolyte composition in 1 M H_2SO_4 + *x* M $HClO_4$ mixtures, they were able to prove that perchlorate associates with ferrocinium more strongly than with bisulfate. They also showed how voltammograms become broadened and displaced toward more positive potentials upon increasing the chain length of the coadsorbed alkanethiol. They neglected double-layer effects and interpreted the influence of the coadsorbate on the basis of a progressive rise of ferrocinium energy as it becomes buried in an alkane environment. A simultaneous broadening and shift of the voltammogram is to be expected on the basis of arguments presented above when the ratio γ_A/ϵ_a increases. Therefore, it seems interesting to see to what extent the present model helps one to rationalize Rowe and Creager's results.

To fit the voltammograms and variations of the peak potential with perchlorate concentration displayed in Figures 11 and 12, the following procedure was adopted.

The distance β from the electrode to the redox centers was fixed at a value of 1.2 nm, corresponding approximately to an *all-trans*-ferrocenyl-*n*-alkanethiol-adsorbed molecule. Although there is the possibility that some conformational folding occurs in the presence of the shortest coadsorbates, thus reducing the effective value of β, results were found to be nearly independent of the precise choice of β in the range $10 \leq \beta \leq 14$ Å.

In addition, the value of ϵ_a was fixed at 6. This is the mean value obtained when the nonfaradaic behavior of the five monolayers was modeled as a plane capacitor, with a coadsorbate dependent thickness estimated as suggested in ref 17. Though this permittivity value is higher than that expected for an alkane environment and probably reflects some solvent and/or ion pemeation through the shortest alkanethiols, it should suffice to illustrate the applicability of our model to a given experimental situation.

Γ_T and the γ_A/ϵ_a ratio were obtained by fitting the faradaic component of the voltammograms recorded in 1 M $HClO_4$, for arbitrary values of ϕ_o^m and K_{OClO_4-}. Under strong ion-pairing conditions, these two last parameters only lead to a displacement of the voltammogram along the potentials axis, without modifying its shape. Individual values of γ_A and ϵ_a are hard to determine from the fit, since they contribute through their ratio to the $\phi^r - \phi^A$ potential drop.

TABLE 1: Parameter Values for the Fits in Figures 11 and 12

coadsorbate	$\Gamma_T \times 10^{11}$ (mol cm^{-2})	$\gamma_A\epsilon_a^{-1}$ (Å)	$\phi_o^{m\,a}$ (V)	$K_{OClO_4^-}{}^a$ (M^{-1})	$K_{OClO_4^-}/K_{OSO_4H^-}{}^b$
HSC_4H_9	3.2	0.083	0.680	180	310
HSC_6H_{13}	2.7	0.10	0.685	180	310
HSC_8H_{17}	3.3	0.13	0.750	600	1300
$HSC_{10}H_{21}$	3.0	0.22	0.815	1100	2200
$HSC_{12}H_{25}$	4.7	0.22	0.850	1700	5400

[a] Lowest limits obtained from the $K_{OSO_4H^-} \geq 0$ condition. [b] Derived from the $K_{OClO_4^-}$, $K_{OSO_4H^-} \geq 10$ M^{-1} assumption.

At this point, K_{OClO_4-} and ϕ_o^m remain undetermined, since one of them is required to obtain the other from the peak potential. To solve this problem, one may adopt for ϕ_o^m the reported value for the water soluble analogue hydroxymethylferrocene 0.21 V (vs Ag/AgCl) or 0.61 V in the rational scale (assuming −0.4 V vs Ag/AgCl for the potential of zero charge of the thiol monolayer[20,21]). Unfortunately, this simple choice of ϕ_o^m turns out to be too negative to reproduce the peak potentials in the presence of 1 M H_2SO_4. To proceed further, we have considered two alternative and complementary hypotheses.

(i) Bisulfate Is Weakly Associated with Ferrocinium ($K_{OSO_4H^-} \leq 1$ M^{-1}). This hypothesis implies that ϕ_o^m can be obtained from the peak potential recorded in the presence of solutions where bisulfate is the only counterion. Once ϕ_o^m is known, K_{OClO_4-} can be determined from the variation of peak potential with perchlorate concentration (Figure 12). It should be stressed again that, because of the previous assumption, these values of ϕ_o^m and K_{OClO_4-}, which are listed in Table 1, should be considered only as lowest limits of the true values. They were obtained by taking $\gamma = \gamma_A$; however, it may be more appropriate to consider $\gamma > \gamma_A$ when the chain length of the coadsorbate is longer than that of the adsorbed redox centers. The presence of a low-permittivity region accessible to counterions leads to ϕ_o^m values that are 40 mV more negative than those in Table 1 and decreases the corresponding association constants by a factor

of 5. In any case, the qualitative trend of these parameters remains the same, that is, they increase with the chain length of the coadsorbate.

In fact, Rowe and Creager interpreted their results assuming that $K_{OSO_4H^-} \leq 0.1\ M^{-1}$, although they did not stated it explicitly. Comparing with their analysis, inclusion of double-layer effects decreases the association constant values, due to a local enhancement of the counterion concentration, and also reduces the range of variation of ϕ_o^m and $K_{OClO_4^-}$ to be ascribed to environmental effects, since that variation can be partially associated to changes in the γ_A/ϵ_a ratio. Moreover, the observed broadening of the voltammetric wave can only be explained if allowance is made for variations in the $\phi^r - \phi^A$ potential drop. Though a consistent account of Rowe and Creager's results can be reached by assuming a weak association between ferrocinium and bisulfate, there seems to be no evidence to discard an alternative starting point based on strong association between these two ions.

(ii) Bisulfate and Perchlorate Strongly Associated with Ferrocinium ($K_{OSO_4H^-}$ and $K_{OClO_4^-} \geq 10\ M^{-1}$). When this hypothesis is adopted, no information becomes available on the absolute values of the formal potential or the association constants, except for the fact that the previous lower limits for these parameters move toward more positive potentials and higher association constants. But still, one can obtain $K_{OClO_4^-}/K_{OSO_4H^-}$ ratios from the peak potential dependence on electrolyte composition (Figure 12). These ratios do not vary for any value of γ greater than or equal to γ_A and are listed in Table 1.

The increase of $K_{OClO_4^-}/K_{OSO_4H^-}$ with coadsorbate chain length is compatible with the physical picture that emerged from the weak association hypothesis, but it opens other possibilities as well. For instance, the changes in the γ_A/ϵ_a and $K_{OClO_4^-}/K_{OSO_4H^-}$ ratios are consistent also with an increase in the distance of closest approach between the ferrocinium centers and the counterions as the coadsorbate chain length is made longer. Then both association constants would be expected to decrease, although $K_{OSO_4H^-}$ would decrease at a faster rate. This type of ambiguity in the analysis of the voltammetric experiments is closely related to the lack of a precise knowledge of either the formal potential of the adsorbed redox couple or the association constant with a given counterion. Whatever starting hypothesis is chosen, some qualitative conclusions can be reached from the above analysis; namely, (a) the formal potential of the adsorbed ferrocinium/ferrocene couple is more positive than that of its water soluble analogue; (b) most ferrocinium sites form ion pairs in the presence of perchlorate; and (c) the ferrocinium−perchlorate association constant increases with respect to that of the ferrocinium−bisulfate ion pair, as the chain length of the coadsorbate is made longer.

The fits displayed in Figures 11 and 12 are quite satisfactory, but there are two features that deserve some further comments. According to plot c in Figure 11, experimental and simulated voltammograms, corresponding to *n*-octanethiol as coadsorbate, are shifted by 30 mV. By noting the location of the 1 M $HClO_4$ peak potential in plot c of Figure 12, it becomes evident that this point lies outside of any reasonable extrapolation of peak potentials reported in ref 4 for the rest of the electrolyte mixtures. Therefore, we conclude that the shift observed in Figure 11 is not related to a failure of the model.

A more interesting question is raised by the fact that the experimental current values are systematically higher than the theoretical ones when the monolayer becomes extensively ionized at positive potentials. This tailing effect, which is more pronounced as the coadsorbate chain length increases, is not predicted by our model. However, preliminary results indicate that this behavior is to be expected when discreteness of charge effects are included in the theoretical description of the monolayer.

SCHEME 2

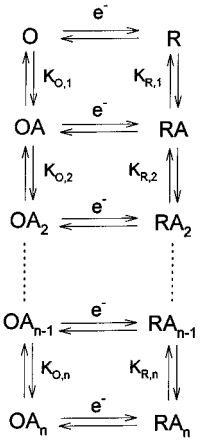

Concluding Remarks

On the basis of the present analysis and data available in the literature, it is clear that ion pairing is an important aspect of the analysis of thermodynamic data for self-assembled monolayers incorporating a redox couple. Double-layer effects for these systems should include a description of the role of ion pairing. In the present paper, these effects have been described on the basis of the traditional model of the double layer which considers only the variation in the average electrostatic potential in a direction perpendicular to the electrode/solution interface. In this sense, the present work represents a direct extension of the earlier work by Smith and White.[1] Preliminary results have indicated that discreteness-of-charge effects[22] can be detected for these systems under certain circumstances. These effects and their consequences for experimental results will be the subject of a future paper.

Acknowledgment. This work was supported by the Spanish DGICYT under Grant PB095-0537. W.R.F. thanks the Office of Naval Research, Washington, for financial support. J.J.C. thanks the Ministerio de Educacion y Ciencia, Spain, for an FPI fellowship.

Appendix A

In this Appendix the theoretical description for the case where the redox couple can participate in *N* association equilibria is derived. Let us consider Scheme 2. The horizontal lines represent electron transfer processes, whereas the vertical ones stand for the ionic association processes.

For a pair of vertical lines *i* under equilibrium conditions, the following is true:

$$\bar{\mu}_{OA_{i-1}} + \bar{\mu}_A = \bar{\mu}_{OA_i} \tag{A.1}$$

$$\bar{\mu}_{RA_{i-1}} + \bar{\mu}_A = \bar{\mu}_{RA_i} \tag{A.2}$$

By using the expressions for the electrochemical potentials given by eqs 3, 14, and 15, eqs A.1 and A.2 are converted into

$$\frac{\theta_{OA_i}}{\theta_{OA_{i-1}}} = K_{O,i} c_A \exp(-z_A F \phi^A / RT) \tag{A.3}$$

$$\frac{\theta_{RA_i}}{\theta_{RA_{i-1}}} = K_{R,i} c_A \exp(-z_A F \phi^A / RT) \tag{A.4}$$

The surface coverages θ_{OAi} and θ_{RAi} can be written as

$$\theta_{OA_i} = \theta_{OA}\prod_{k=2}^{i}\frac{\theta_{OA_k}}{\theta_{OA_{k-1}}} \quad (A.5)$$

$$\theta_{RA_i} = \theta_{RA}\prod_{k=2}^{i}\frac{\theta_{RA_k}}{\theta_{RA_{k-1}}} \quad (A.6)$$

Substituting eqs A.3 and A.4 into eqs A.5 and A.6, one obtains

$$\theta_{OA_i} = \theta_R\rho\lambda_{O,i} \quad (A.7)$$

$$\theta_{RA_i} = \theta_R\lambda_{R,i} \quad (A.8)$$

where ρ represents the ratio θ_O/θ_R (see eq 33) and $\lambda_{X,i}$ is defined as

$$\lambda_{X,i} = c_A^i \exp(-iz_AF\phi^A/RT)\prod_{k=1}^{i}K_{X,k} \qquad (X \equiv O, R) \quad (A.9)$$

Γ_T represents the sum, per unit area, of all species involved in the electron transfer processes, and therefore

$$\theta_O + \theta_R + \sum_{k=1}^{N}\theta_{OA_k} + \sum_{k=1}^{N}\theta_{RA_k} = 1 \quad (A.10)$$

Combining eqs A.7, A.8, and A.10, one obtains

$$\theta_R = \frac{1}{1 + \rho + \sum_{i=1}^{N}(\lambda_{R,i} + \rho\lambda_{O,i})} \quad (A.11)$$

Substituting eq A.11 into eqs 31, A.7, and A.8, the following expressions for the surface coverages of O, OA_i, and RA_i result

$$\theta_O = \frac{\rho}{1 + \rho + \sum_{i=1}^{N}(\lambda_{R,i} + \rho\lambda_{O,i})} \quad (A.12)$$

$$\theta_{RA_i} = \frac{\lambda_{R,i}}{1 + \rho + \sum_{i=1}^{N}(\lambda_{R,i} + \rho\lambda_{O,i})} \quad (A.13)$$

$$\theta_{OA_i} = \frac{\rho\lambda_{O,i}}{1 + \rho + \sum_{i=1}^{N}(\lambda_{R,i} + \rho\lambda_{O,i})} \quad (A.14)$$

The charge density at the plane defined by the redox centers is given by

$$\sigma_r = F\Gamma_T\{z_O(\theta_O + \sum_{i=1}^{N}\theta_{OA_i}) + z_R(\theta_R + \sum_{i=1}^{N}\theta_{RA_i})\} \quad (A.15)$$

and that at the plane $x = x_A$ due to the associated counterions is

$$\sigma_A = z_AF\Gamma_T\sum_{i=1}^{N}i(\theta_{OA_i} + \theta_{RA_i}) \quad (A.16)$$

By substituting eqs A.11−A.14 into eqs A.15 and A.16, one obtains

$$\sigma_r = F\Gamma_T\frac{z_O\rho + z_R + \sum_{i=1}^{N}(z_O\rho\lambda_{O,i} + z_R\lambda_{R,i})}{1 + \rho + \sum_{i=1}^{N}(\lambda_{R,i} + \rho\lambda_{O,i})} \quad (A.17)$$

$$\sigma_a = F\Gamma_Tz_A\frac{\sum_{i=1}^{N}i(\rho\lambda_{O,i} + \lambda_{R,i})}{1 + \rho + \sum_{i=1}^{N}(\lambda_{R,i} + \rho\lambda_{O,i})} \quad (A.18)$$

For a given set of the parameters which characterize the system, the above equations are solved numerically as follows: (1) A value of σ_m is selected and ρ is calculated by using eq 23. (2) An initial value of ϕ^A is assumed as the first step of the iterative process. For instance, ϕ^A can be set equal to zero. (3) The charge densities (σ_r and σ_a) and the surface coverages of the different species $\{\theta_i\}$ are calculated by using eqs A.17, A.18, and A.11−A.14, respectively. (4) With the results from step 3, an improved estimate of ϕ^A is calculated by using eq 24 or eqs 25−30 depending on whether the counterion can or cannot enter the outer part of the SAM. (5) Steps 3 and 4 are iteratively repeated until a convergence in the values of $\{\theta_i\}$ is reached.

Supporting Information Available: Derived working equations for the case that two counterions can form ion pairs along with Scheme B.1. showing their formations (4 pages). Ordering information is given on any current masthead.

References and Notes

(1) Smith, C. P.; White H. S. *Anal. Chem.* **1992**, *64*, 2398.

(2) Smith, C. P.; White H. S. *Langmuir* **1993**, *9*, 1.

(3) Creager, S. E.; Rowe, G. K. *Anal. Chim. Acta* **1991**, *246*, 233.

(4) Rowe, G. K.; Greager, S. E. *Langmuir* **1991**, *7*, 2307.

(5) Rowe, G. K.; Creager, S. E. *J. Phys. Chem.* **1994**, *98*, 5500.

(6) De Long, H. C.; Donohue J. J.; Buttry, D. A. *Langmuir* **1991**, *7*, 2196.

(7) Shimazu, K.; Yagi, I.; Sato, Y.; Uosaki, K. *J. Electroanal. Chem.* **1994**, *372*, 117.

(8) De Long, H. C.; Buttry, D. A. *Langmuir* **1992**, *8*, 2491.

(9) Redepenning, J.; Flood, J. M. *Langmuir* **1996**, *12*, 508.

(10) Redepenning, J.; Tunison, H. M.; Finklea, H. O. *Langmuir* **1993**, *9*, 1404.

(11) Acevedo, D.; Abrun⁻a, H. D. *J. Phys. Chem.* **1991**, *95*, 9590.

(12) Ulman, A. *An Introduction to Ultrathin Organic Films: From Langmuir-Blodgett to Self-Assembly*; Academic Press: San Diego, 1991.

(13) Bard, A. J.; Faulkner, L. R. *Electrochemical Methods*; J. Wiley: New York, 1980.

(14) Valleau, J. P.; Torrie, G. M. *J. Chem. Phys.* **1982**, *76*, 4623.

(15) Andreu, R.; Molero, M.; Calvente, J. J.; Carbajo, J. *J. Electroanal. Chem.* **1993**, *358*, 49.

(16) Collins, W. R.; Allara, D. L.; Kim, Y.; Lu, Y.; Shi, J. In *Characterization of Organic Films*; Ulman, A., Ed.; Butterworth-Heinemann, Stoneham, 1995.

(17) Porter, M. D.; Bright, B. T.; Allara, D. L.; Chidsey, C. E. D. *J. Am. Chem. Soc.* **1987**, *109*, 3559.

(18) Laviron, E. *J. Electroanal. Chem.* **1974**, *52*, 355, 395.

(19) Albert, A.; Serjeant, E. P. *Ionization Constants of Acids and Bases*; Butler and Tauner: London, 1962.

(20) Becka, A. M.; Miller, C. J. *J. Phys. Chem.* **1993**, *97*, 6233.

(21) Sondag-Huethorst, J. A. M.; Fokkink, L. G. J. *J. Electroanal. Chem.* **1994**, *367*, 49.

(22) Fawcett, W. R. *J. Electroanal. Chem.* **1994**, *378*, 117.